International Journal of Thermophysics, Vol. 24, No. 5, September 2003 (© 2003)

Thermophysical Properties of the Refrigerant Mixtures R410A and R407C from Dynamic Light Scattering (DLS)[1]

A. P. Fröba[2,3] and A. Leipertz[2]

Dynamic light scattering (DLS) has been used for the measurement of several thermophysical properties of the refrigerant mixtures R410A and R407C. Thermal diffusivity and sound speed have been obtained by light scattering from bulk fluids for both the liquid and vapor phases under saturation conditions over a temperature range from about 290 K up to the liquid-vapor critical point. By applying the method of DLS to a liquid-vapor interface, also called surface light scattering (SLS), the saturated liquid kinematic viscosity and surface tension can be determined simultaneously. These properties have been measured for R410A and R407C from about 240 to 330 K and 240 to 350 K, respectively. The results are discussed in detail in comparison with literature data and with a simple prediction method based on the mass-weighted properties of the pure components expressed as functions of the reduced temperature.

KEY WORDS: dynamic light scattering; kinematic viscosity; R407C; R410A; sound speed; surface light scattering; surface tension; thermal diffusivity.

1. INTRODUCTION

In recent years intensive international activities have been carried out in order to rapidly provide comprehensive data sets for the thermophysical properties of all possibly relevant substitutes for the fully-halogenated hydrocarbons used previously. Because of their thermodynamic properties and of safety requirements, chlorine-free HFCs, except for R23 and R134a

[1] Paper presented at the Sixteenth European Conference on Thermophysical Properties, September 1–4, 2002, London, United Kingdom.

[2] Lehrstuhl für Technische Thermodynamik (LTT), Friedrich-Alexander-Universität Erlangen-Nürnberg, Am Weichselgarten 8, D-91058 Erlangen, Germany.

[3] To whom correspondence should be addressed. E-mail: apf@ltt.uni-erlangen.de

0195-928X/03/0900-1185/0 © 2003 Plenum Publishing Corporation

which are used as direct substitutes for R13 and R12, respectively, are employed as mixtures in almost all fields of refrigeration and air conditioning. A literature survey reveals that, in contrast to the pure substances, only a very limited number of experimental data are available for mixtures from the group of partially fluorinated hydrocarbons. This situation holds for equilibrium data and is even more pronounced for transport properties.

The present work represents an extension of a study by dynamic light scattering for refrigerant mixtures of technical interest, where (on a mass basis) the binary and ternary mixture R507 (50% R125/50% R143a) and R404A (52% R143a/44% R125/4% R134a), respectively, already have been investigated [1]. It is the major aim of this work to contribute to the verification and improvement of the data situation for the binary near-azeotropic mixture R410A (50% R125/50% R32) and for the ternary zeotropic mixture R407C (25% R125/23% R32/52% R134a), which are most favored worldwide as long-term alternatives for R22 (chlorodifluoromethane) in new plants in the field of compact air conditioning and heat pump systems [2].

In the present paper, first, the methodological principles of dynamic light scattering (DLS) for the determination of thermal diffusivity, sound speed, kinematic viscosity, and surface tension are briefly reviewed. Then, the experimental results for R410A and R407C are presented and compared with the few literature data available and with a simple prediction method based on the properties of the pure components.

2. METHOD

Dynamic light scattering is a unique diagnostic tool for the determination of a variety of thermophysical properties of fluids using a basically identical experimental setup. In contrast to conventional methods, most of which are working with macroscopic gradients according to the desired quantities, DLS provides information on thermophysical properties of fluids in macroscopic thermodynamic equilibrium. In the following, the underlying theory of dynamic light scattering (DLS) from bulk fluids and the application of this method to fluid surfaces also called surface light scattering (SLS) is briefly introduced. For a more detailed and comprehensive description the reader is referred to the specialized literature [3–5].

2.1. Principle of Light Scattering from Bulk Fluids

When a fluid sample in macroscopic thermodynamic equilibrium is irradiated by coherent laser light, light scattered from the sample can be observed in all directions. The underlying scattering process is governed by

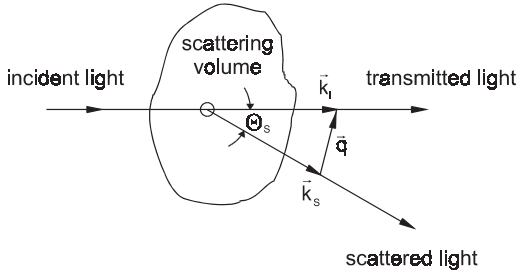

Fig. 1. Scattering geometry: light scattering from bulk fluids.

microscopic fluctuations of temperature (or entropy), of pressure, and of species concentration in mixtures. The relaxations of these statistical fluctuations follow the same rules that are valid for the relaxation of macroscopic systems. Thus, the decay of temperature fluctuations is governed by the thermal diffusivity a. Pressure fluctuations in fluids are moving with a sound speed u_S and their decay is governed by the sound attenuation D_S. In a binary fluid mixture the decay of concentration fluctuations is governed by the mutual diffusion coefficient D_{12}.

A typical scattering geometry for light scattering from bulk fluids is shown in Fig. 1. With the scattering angle Θ_S, which defines the angle between the direction of observation and incident light, the scattering vector is determined by $\vec{q} = \vec{k}_I - \vec{k}_S$. Here, the wave vectors of incident and scattered light are represented by $\vec{k}_I$ and $\vec{k}_S$, respectively. Assuming elastic scattering ($k_I \cong k_S$), the modulus of the scattering vector is given by the fluid refractive index n, the laser wavelength in vacuo λ_0, and the scattering angle Θ_S by

$$q = |\vec{k}_I - \vec{k}_S| \cong 2k_I \sin(\Theta_S/2) = \frac{4\pi n}{\lambda_0} \sin(\Theta_S/2). \tag{1}$$

In light scattering experiments the above-mentioned equalization processes result in a temporal modulation of the scattered light intensity. Information about these processes can be derived through a temporal analysis of the scattered light intensity by using photon correlation spectroscopy (PCS). For heterodyne conditions, where the scattered light is superimposed with stronger coherent reference light, the time-dependent intensity correlation function for the analysis of the temperature fluctuations is described by

$$G^{(2)}(\tau) = A + B \exp(-\tau/\tau_C) \tag{2}$$

where A and B are experimental constants, which are essentially determined by total number of counts registered, the ratio of scattered light to reference light, and the coherence properties of the optical system. From the correlation time τ_C, which is equivalent to the mean life time of the temperature fluctuations observed, the thermal diffusivity a can be calculated by

$$a = \frac{1}{\tau_C q^2}. \tag{3}$$

For the measurement of sound speed u_S the pressure fluctuations are probed. In practice, the frequency ω_S of the sound waves is determined by adding a reference beam, which is shifted relative to the frequency ω_0 of the laser light by $\Delta\omega_M$ applying an acousto-optical modulator. The frequency shift $\Delta\omega_M$ is of the same order of magnitude as the frequency of the sound waves ($\Delta\omega_M \approx \omega_S$). In this case, the correlation function takes the form,

$$G^{(2)}(\tau) = A + B \exp(-\tau/\tau_C) \cos(\Delta\omega\tau), \tag{4}$$

and the sound speed u_S can be found from a knowledge of the adjusted modulator frequency $\Delta\omega_M$ and the residual detuning $\Delta\omega$ according to

$$u_S = \frac{\omega_S}{q} = \frac{\Delta\omega_M \pm \Delta\omega}{q}. \tag{5}$$

Furthermore, the sound attenuation D_S can be determined from the decay time τ_C of the correlation function Eq. (4) by

$$D_S = \frac{1}{\tau_C q^2}. \tag{6}$$

Whether it is possible to determine signals from concentration fluctuations is mainly governed by the relative difference of the refraction indices of the mixture components and their concentration. For the refrigerant mixtures studied in this work the refractive indices of the pure components have comparable values [6–8]; thus, the scattered light signals from only temperature and pressure fluctuations associated with thermal diffusivity and sound speed can be resolved, respectively.

2.2. Principle of Surface Light Scattering (SLS)

Liquid-vapor interfaces in macroscopic thermal equilibrium exhibit surface waves which are caused by thermal movement of molecules and

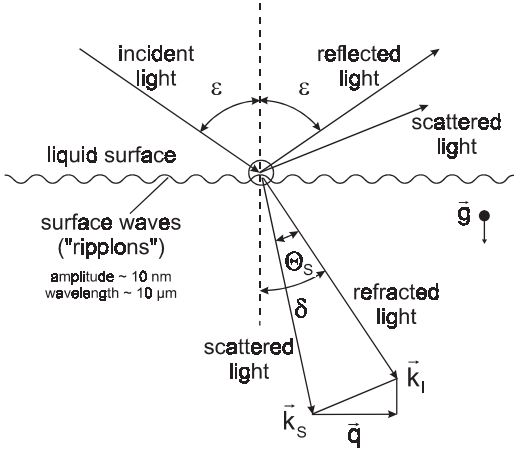

Fig. 2. Scattering geometry: light scattering by surface waves.

which are quantized in so-called "ripplons." For small viscosities, as is relevant in the experiments described here, the amplitude of surface waves decays in the form of a damped oscillation. SLS analyzes the light scattered by these surface waves.

With the surface light scattering geometry used in this work, scattered light is observed in the forward direction near refraction; see Fig. 2. By the choice of the angle of incidence ε, resulting in a specific angle δ of the refracted light, and the scattering angle Θ_S, the scattering vector $\vec{q} = \vec{k}'_I - \vec{k}'_S$ is determined and, from this, the wave vector and frequency of the observed surface vibration mode. Here, $\vec{k}'_I$ and $\vec{k}'_S$ denote the projections of the wave vectors of the refracted ($\vec{k}_I$) and scattered light ($\vec{k}_S$) in the surface plane, respectively. For the observation of scattered light within the irradiation plane and assuming elastic scattering (i.e., $k_I \cong k_S$), the modulus of the scattering vector is expressed as

$$q = |\vec{k}'_I - \vec{k}'_S| \cong 2k_I \sin(\Theta_S/2) \cos(\delta - \Theta_S/2)$$
$$= \frac{4\pi n}{\lambda_0} \sin(\Theta_S/2) \cos(\delta - \Theta_S/2), \quad (7)$$

where again n is the fluid refractive index and λ_0 is the laser wavelength in vacuo.

In the case of large heterodyning, the correlation function of light scattered by surface fluctuations may be described by

$$G^{(2)}(\tau) = A + B \cos(\omega_R |\tau| - \phi) \exp(-|\tau|/\tau_C), \quad (8)$$

where the phase term ϕ, $\phi = \text{atan}(\Gamma/\omega_R)$, largely accounts for the deviations of the power spectrum of the surface fluctuations from the Lorentzian form and the correlation time τ_C and the frequency ω_R are identical with the mean life time or the reciprocal of the damping constant Γ $(= 1/\tau_C)$ of "ripplons" and the frequency of propagation, respectively. The latter relate to the fluid properties of the liquid-vapor interface through the capillary wave dispersion equation,

$$\left\{[\mathrm{i}\alpha(\eta' m' + \eta' q + \eta'' m'' + \eta'' q)]\left[\sigma q^2 + \mathrm{i}\alpha(\eta' m' + \eta' q + \eta'' m'' + \eta'' q) + g(\rho' - \rho'') - \frac{\alpha^2}{q}(\rho' + \rho'')\right] - [\mathrm{i}\alpha(\eta' q - \eta' m' + \eta'' m'' - \eta'' q)]^2\right\} = 0, \tag{9}$$

where

$$\alpha = \omega_R + \mathrm{i}\Gamma, \tag{10}$$

$$m' = \sqrt{q^2 + \mathrm{i}\frac{\alpha\rho'}{\eta'}}, \qquad m'' = \sqrt{q^2 + \mathrm{i}\frac{\alpha\rho''}{\eta''}}, \tag{11}$$

g is the acceleration of gravity, σ is the surface tension, ρ' and ρ'' are the densities of the liquid and vapor phases, respectively, and η' and η'' are the dynamic viscosities of the liquid and vapor phases, respectively. This complex relation is the result of the solution of the linearized Navier–Stokes equation whereby the fluid flow must satisfy boundary conditions that express the continuity of normal and tangential stresses at the liquid-vapor interface.

To a first-order approximation, the ratio of the sum of the dynamic viscosities of the liquid and vapor phase relative to the sum of the densities of the liquid and vapor phase may be obtained from the decay time τ_C of the correlation function Eq. (8) by

$$\frac{\eta' + \eta''}{\rho' + \rho''} \approx \frac{1}{2\tau_C q^2}. \tag{12}$$

Furthermore, the correlation function Eq. (8) can simultaneously be evaluated for the ratio of the surface tension to the sum of the densities of the vapor and liquid phase,

$$\frac{\sigma}{\rho' + \rho''} \approx \frac{\omega_R^2}{q^3}, \tag{13}$$

which, to a first-order approximation, follows directly from the beat frequency ω_R and the modulus of the wave vector q.

For a reliable determination of viscosity and surface tension, a more detailed and rigorous consideration of the surface light scattering method than given by Eqs. (12) and (13) has to be applied. In the present work, however, data for the liquid kinematic viscosity and surface tension were obtained by an exact numerical solution of the dispersion equation for surface waves at a liquid-vapor interface, Eq. (9), where the measured frequency ω_R, the damping Γ, and the modulus of the wave vector q are used as input values.

3. EXPERIMENTAL

The optical and electro-optical parts of the experimental setup used for the determination of sound speed and thermal diffusivity are shown—in a top view—on the left side of Fig. 3. For performing light scattering from bulk fluids, the scattering volume, which is determined by the intersection of the incident beam and the axis of observation (dashed line), is located in the middle of the vessel. The principle of the scattering geometry which allows scattering by surface waves is shown schematically—in a front view—on the right side of Fig. 3. In this case, the optical path has to be aligned in such a way that the laser beam and the direction of detection intersect on the liquid-vapor interface in the measurement cell. The basic modification of the setup on the left side of Fig. 3 for the realization of surface light scattering experiments was to mount the pressure vessel in a vertical position.

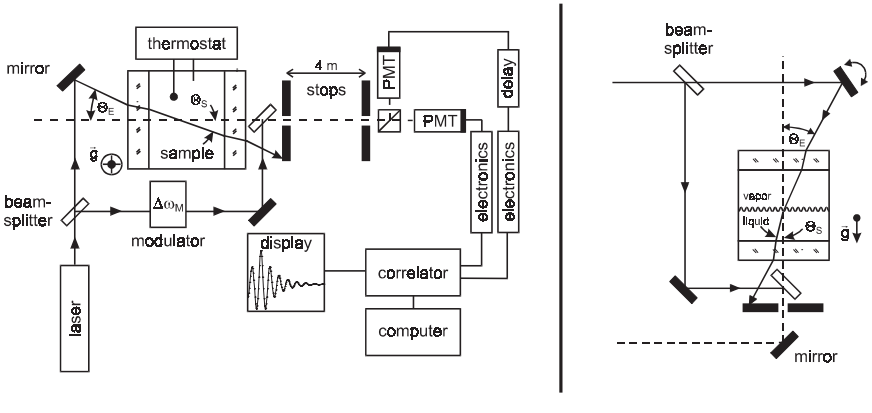

Fig. 3. Experimental setup: optical and electronic arrangement.

As a light source, an argon ion laser ($\lambda_0 = 488$ nm) and a frequency doubled continuous wave Nd:YVO_4-laser ($\lambda_0 = 532$ nm) were optionally used. The laser power was up to 300 mW when working far away from the critical point, and only a few mW in the critical region. For large scattering intensities, scattered reference light from the cell windows alone is not sufficient to realize heterodyne conditions. Here, an additional reference beam is added. To this end, part of the incident laser light is split by a glass plate and superimposed with the scattered light behind the sample cell. For the determination of sound speed, a reference beam shifted in frequency by an opto-acoustic modulator was added to the scattered light. The time-dependent intensity of the scattered light is detected by two photomultiplier tubes (PMT's) operated in cross-correlation in order to suppress after-pulsing effects. The signals are amplified, discriminated, and fed to a digital correlator.

With the help of Snell's refraction law and simple trigonometric identities, it can be shown that for both light scattering from bulk fluids and light scattering by surface waves, the scattering vector q can be deduced as a function of the easily accessible angle of incidence Θ_E, which is defined, see Fig. 3, as the angle between the optical axis of the incident laser beam and the detection direction,

$$q = \frac{2\pi}{\lambda_0} \sin(\Theta_E). \tag{14}$$

For light scattering from bulk fluids, Eq. (14) represents a good approximation for the determination of the modulus of the scattering vector without a knowledge of the refractive index n of the sample, where the error in q is less than 0.1% for scattering angles up to 5°. In the surface light scattering experiments described here, the scattered light is detected perpendicular to the liquid-vapor interface, which means $\Theta_S = \delta$; see Fig. 2. For this arrangement the modulus of the scattering vector is obtained exactly from Eq. (14).

For the measurement of the angle of incidence Θ_E, the laser beam is first adjusted through the detection system consisting of two apertures ($\varnothing$ 1 to 2 mm) at a distance of about 4 m. Then the laser beam is set to the desired angle. For the experiment the angle of incidence Θ_E was set between 3.0 and 6.0° and was measured with a high precision rotation table. The errors in the angle measurement have been determined to be approximately ± 0.005 and ± 0.014° for the observation of light scattered by surface waves and from bulk fluids, respectively. In both cases the error in the angle measurement results in a maximum uncertainty of less than 1% for the desired thermophysical properties.

According to the specifications of the manufacturer (Solvay Fluor & Derivate GmbH, Hannover), the refrigerant mixtures had a purity of $\geqslant 99.5\%$ and were used without further purification. The composition (on a mass basis) for the near-azeotropic mixture R410A is certified to be in a range from 49.5 to 51.5% for R125 and from 48.5 to 50.5% for R32. The ternary mixture R407C consists of 51% R134a, 26% R125, and 23% R32, where the uncertainty in the composition is certified to be $\pm 2\%$ for each component. For the present measurements, the samples were filled into an evacuated cylindrical pressure vessel (volume $\approx 10\ \mathrm{cm}^3$) from the liquid phase to avoid decomposition, which is relevant, in particular, for the refrigerant mixture R407C, which represents a zeotropic mixture. For this reason investigations for R407C were restricted to the liquid phase, and special experimental care has been exercised to maintain the mixture at the certified composition of the manufacturer for the complete temperature range investigated. In order to keep the change in composition to a minimum, the vapor space had to be kept as small as possible in the measuring cell.

The temperature of the pressure vessel, which is placed inside an insulated housing, is regulated through resistance heating and measured by calibrated 25-Ω or 100-Ω platinum resistance probes with an uncertainty of ± 0.015 K. The temperature stability was better than ± 0.002 K during a single experimental run. For each temperature point, typically six measurements at different angles of incidence were performed, where the laser was irradiated from either side with respect to the axis of observation in order to check for a possible misalignment. For temperatures below room temperature, the insulating housing was cooled to about 10 K below the desired temperature in the sample cell by a lab thermostat. The measurement times for a single run were typically of the order of ten minutes down to a few seconds for the highest temperatures in this study. A more detailed description of the experimental setups can be found in Refs. 9–11.

4. RESULTS AND DISCUSSION

4.1. Thermal Diffusivity and Sound Speed

The experimental data for the thermal diffusivity and sound speed of R410A and R407C obtained by light scattering from bulk fluids are summarized in Tables I and II. In Figs. 4 and 5, besides the mixture data, the pure component data are also shown, which have been taken from previous investigations [12–15]. The continuous lines are empirical correlations of the experimental data. For the mixtures each temperature point comprises six single measurements, the mean value of which is displayed. For reduced

Table I. Experimental Values of the Thermal Diffusivity a of R410A and R407C Under Saturation Conditions

R410A				R407C	
Liquid phase		Vapor phase		Liquid phase	
T (K)	a (10^{-8} m$^2\cdot$s^{-1})	T (K)	a (10^{-8} m$^2\cdot$s^{-1})	T (K)	a (10^{-8} m$^2\cdot$s^{-1})
298.14	4.69	315.63	9.75	293.16	4.61
303.14	4.44	318.13	8.81	298.17	4.47
308.13	4.24	320.63	8.00	303.17	4.31
313.13	4.03	323.12	7.12	308.16	4.23
318.13	3.74	325.63	6.35	313.16	4.05
323.12	3.44	328.12	5.46	318.16	3.86
325.62	3.23	330.62	4.63	323.14	3.66
328.13	3.05	333.12	3.83	328.14	3.46
330.62	2.80	335.61	3.03	333.13	3.25
333.14	2.54	338.11	2.19	338.12	2.96
335.61	2.22	340.11	1.53	343.12	2.68
338.14	1.80	342.11	0.821	348.11	2.27
340.15	1.38	343.11	0.441	351.10	1.96
342.17	0.809			353.09	1.67
343.16	0.443			354.09	1.52
				356.09	1.16
				357.08	0.944
				358.08	0.679
				359.08	0.357

temperatures $T_R = T/T_C < 0.99$, where T is the absolute temperature and T_C is the critical temperature, the uncertainties of the measured mixture data can be estimated to be less than $\pm 1\%$ for the thermal diffusivity and less than $\pm 0.5\%$ for the sound speed. For the highest temperatures studied in this work, the measurement uncertainty for the thermal diffusivity and sound speed increases to about ± 2 and $\pm 1\%$, respectively. The reason for this behavior can be found by an increasing experimental complexity in the critical region. Of course, the overall uncertainty of our mixture data including the uncertainty in the composition is clearly larger. This effect could be estimated with the help of a simple prediction method which is described in detail below. The uncertainty in the composition may result in an additional uncertainty up to a maximum of ± 0.6 and $\pm 1.2\%$ for the thermal diffusivity of R410A and R407C, respectively. A maximum uncertainty of ± 0.6 and $\pm 1.0\%$ introduced by the uncertainty in the composition could be estimated for the sound speed of R410A and R407C, respectively.

Table II. Experimental Values of the Sound Speed u_S of R410A and R407C under Saturation Conditions

R410A				R407C	
Liquid phase		Vapor phase		Liquid phase	
T (K)	u_S ($m \cdot s^{-1}$)	T (K)	u_S ($m \cdot s^{-1}$)	T (K)	u_S ($m \cdot s^{-1}$)
298.14	432.1	315.63	149.7	293.14	495.3
303.14	404.2	318.13	147.6	298.15	469.5
308.13	374.9	320.63	146.0	303.17	446.5
313.13	346.3	323.12	143.7	308.17	421.1
318.13	315.5	325.62	141.7	313.16	394.7
323.12	282.4	328.12	139.0	318.15	369.9
325.63	264.8	330.62	136.5	323.15	342.1
328.13	248.0	333.12	133.6	328.14	314.5
330.62	230.0	335.61	130.6	333.13	286.0
333.14	211.7	338.11	126.4	338.12	256.7
335.61	191.7	340.11	123.2	343.12	225.6
338.14	170.2	342.11	117.7	348.11	193.0
340.15	151.2	343.11	113.4	351.10	171.7
342.17	127.6			353.09	156.2
343.16	112.4			354.09	148.3
				356.08	132.6
				357.08	123.7
				358.08	114.2
				359.08	103.8

The experimental data for the thermal diffusivity of R410A and R407C for both the vapor and liquid phases under saturation conditions can be represented by the sum of a polynomial and an additional necessary term which explicitly accounts for the critical behavior,

$$a = \sum_{i=0}^{3} a_i (T/\mathrm{K})^i + a_4 (1 - T_R)^{0.67}, \tag{15}$$

where for R410A the critical temperature $T_C = 344.08\ \mathrm{K} \pm 0.05\ \mathrm{K}$ was determined in our measurements by the observation of the vanishing meniscus between liquid and vapor phases when approaching the critical point. A critical temperature of 359.9 K was estimated for R407C by a mass-weighted sum of the critical temperatures of the pure components [16, 17], which is specifically applicable to hydrocarbon mixtures [18]. For either phase the sound speed under saturation conditions may be

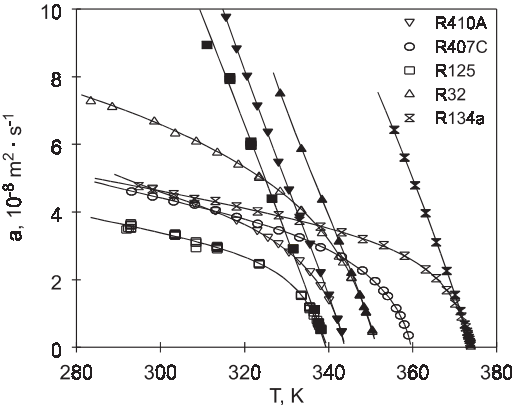

Fig. 4. Thermal diffusivity of saturated R410A and R407C in comparison with the values of the pure components R134a [12], R125 [13], and R32 [14]; open symbols: liquid; filled symbols: vapor.

described by a linear correlation with an additional term to account for the curvature towards the critical point,

$$u_S = u_0 + u_1(T/\mathrm{K}) + u_2(1-T_R)^{\varphi}, \tag{16}$$

where φ represents an additional adjustable parameter. The coefficients for the data correlations determined from our experimental results by least-squares fits are given for thermal diffusivity and sound speed in Tables III

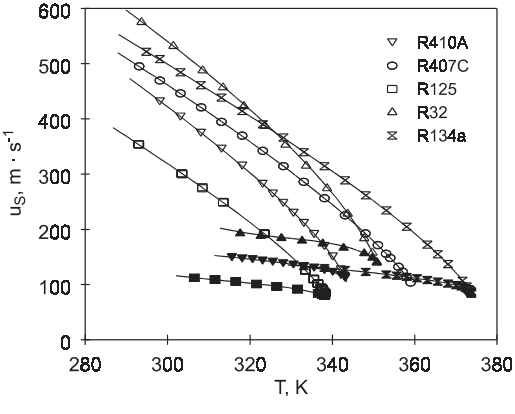

Fig. 5. Speed of sound of saturated R410A and R407C in comparison with the values of the pure components R134a [12], R125 [13], and R32 [15]; filled symbols: vapor; open symbols: liquid.

Table III. Coefficients of Eq. (15) for R410A and R407C

	R410A		R407C
a_i (10^{-8} m$^2 \cdot$ s^{-1})	Liquid phase	Vapor phase	Liquid phase
a_0	230.0137	242.2271	−9.24705
a_1	−2.3964822	−1.2029119	−0.112308
a_2	7.629341×10^{-3}	1.449629×10^{-3}	3.81275×10^{-4}
a_3	-7.584735×10^{-6}	–	–
a_4	46.255	14.650	43.3748
rms (%)	0.88	0.35	0.70
T-range (K)	298–343	316–343	293–359

and IV, respectively. Here, the root-mean square deviations of our values from the correlations and their ranges of validity are stated. Each of these correlations represents the data within experimental uncertainty.

In order to predict the mixture data for thermal diffusivity and sound speed on the basis of the pure component data within the range investigated, we tried several different approaches using, e.g., simple weighting by the mass fractions or the mole fractions of the pure components. In all these cases, remarkable deviations appeared in the vicinity of the critical point when plotting the data against temperature. However, with properties based on the reduced temperature, agreement was found between the measured data and the predicted values when weighting with the mass fractions. The agreement was not this good when using the mole fractions. The properties of the mixture Y_M under saturation conditions have thus been predicted according to

$$Y_M(T_R) = \sum_j w_j Y_j(T_R), \tag{17}$$

Table IV. Coefficients of Eq. (16) for R410A and R407C

	R410A		R407C
u_i (m $\cdot$ s^{-1})	Liquid phase	Vapor phase	Liquid phase
u_0	1245.06	203.601	−43.67
u_1	−3.3672	−0.31589	0.3757
u_2	566.46	90.416	1673
φ	0.539	0.2726	0.8085
rms (%)	0.22	0.12	0.17
T-range (K)	298–343	315–343	293–359

where w_j and Y_j are the mass fraction and the property at the reduced temperature $T_R = T/T_C$ of component j, respectively. The successful application of Eq. (17) requires an accurate knowledge of the mixture critical temperature. If this is not available, significant errors may be introduced by the model especially in approaching the vapor-liquid critical point. For example, in using Eq. (17) for predictions of the thermal diffusivity and sound velocity of R410A in the saturated liquid phase, the root-mean-square deviations of our experimental data from the predictions are kept to minimum values of 4 and 2%, respectively, if the exact value is applied for the critical temperature. However, only a change in the critical temperature by an amount of 0.5 K yields an increase of the root-mean-square deviations by a factor of two.

In Figs. 6 and 7 the experimental results for thermal diffusivity and sound speed, respectively, are compared with this simple prediction method. To this end, the pure component data for thermal diffusivity and sound speed were taken from previous investigations [12–15]. As can be seen from the deviation plots, with the exception for the thermal diffusivity of R407C the predictions are very good with deviations typically smaller than 1% for the sound speed and smaller than 2 to 5% for the thermal diffusivity. Discrepancies between the predicted and experimental values for

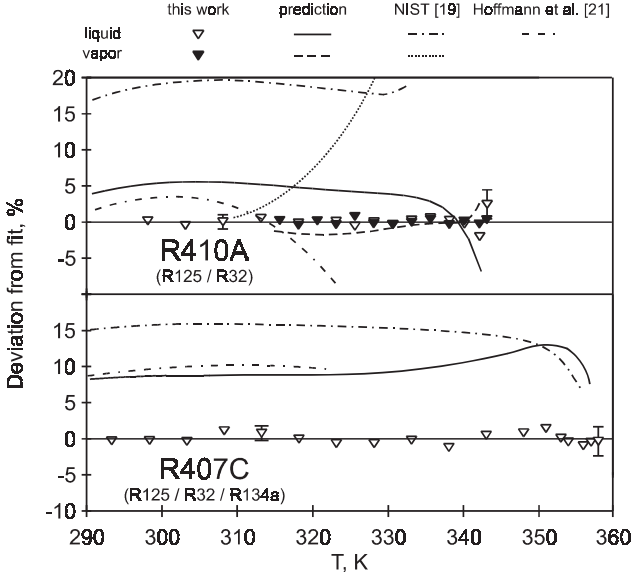

Fig. 6. Data comparisons for the thermal diffusivity of the liquid and vapor phases under saturation conditions for the binary mixture R410A and ternary mixture R407C.

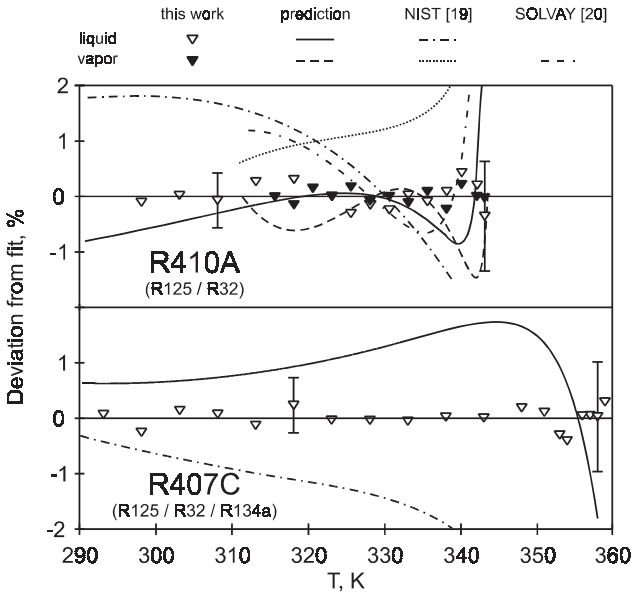

Fig. 7. Data comparisons for the sound speed of the liquid and vapor phases under saturation conditions for the binary mixture R410A and ternary mixture R407C.

the thermal diffusivity of R407C in the liquid phase may be attributed to different curvatures for the pure components. As displayed in Fig. 4, data for the thermal diffusivity of R134a in the liquid phase intersect those of R32.

In Figs. 6 and 7, also included are mixture data from reference databases [19, 20] and the experimental work of Hoffmann et al. [21]. For the latter, data for the liquid thermal conductivity λ obtained by the transient hot-wire method have been converted to thermal diffusivity ($a = \lambda\rho^{-1}c_P^{-1}$) by using reference values for the specific heat at constant pressure c_P of Günther and Steimle [22] and for the density ρ from the SOLVAY database [20]. For R410A the thermal conductivity data of Hoffmann et al. [21] deviate from our correlation in a range of about -5 to $+3.5\%$. These differences are within the combined uncertainties of the methods, if one takes into account the uncertainty of the heat capacity data of less than 1% for temperatures up to 313 K and less than 2% for the temperature range between 313 to 323 K, according to Ref. 22. In contrast, for R407C the deviations between our measurements and the converted data set of Hoffmann et al. [21] are partly larger than 10%, which exceeds the combined estimated uncertainties.

4.2. Kinematic Viscosity and Surface Tension

Data obtained from surface light scattering for the dynamics of surface waves, i.e., frequency ω_R and damping Γ $(=1/\tau_C)$ at a defined wave vector q, have been combined with reference data [19] for the dynamic viscosity of the vapor phase η'' and density data for both phases ρ' and ρ'' to get information about the liquid kinematic viscosity ν' and surface tension σ. Taking into account the uncertainties of the individual quantities entering into the calculation, the uncertainty of our liquid kinematic viscosity data is estimated to be better than $\pm 1\%$ for reduced temperatures $T_R < 0.8$. The uncertainty is clearly larger at higher temperatures, yet for temperatures not too close to the critical point ($T_R < 0.95$), a reasonable value of better than $\pm 2\%$ could be maintained. It should be noted that even approximate values for the dynamic viscosity of the vapor phase are sufficient to achieve such an accuracy. For the existing surface tension data the uncertainty is estimated to be better than $\pm 1.2\%$ for the whole temperature range. A more detailed discussion regarding the accuracy achievable for liquid kinematic viscosity and surface tension from surface light scattering can be found in Refs. 10 and 11. For evaluation of the overall uncertainty of the present mixture data from surface light scattering also the uncertainty in composition has to be taken into consideration. By the use of the model given by Eq. (17), for the kinematic viscosity of R410A and R407C an additional uncertainty up to a maximum of ± 0.2 and $\pm 0.4\%$, respectively, introduced by the uncertainty in the composition could be estimated. From the uncertainty in the composition results for the surface tension of R410A and R407C an additional uncertainty up to a maximum of ± 0.3 and $\pm 0.6\%$, respectively.

The results for the liquid kinematic viscosity and surface tension of R410A and R407C under saturation conditions obtained simultaneously from surface light scattering are summarized in Table V, where values from the literature [19] used for data evaluation, as described above, are also listed. In addition to the mixture data, the pure component data of R134a, R125, and R32, which are reported in Refs. 11 and 23, are also shown in Figs. 8 and 9.

While a simple or modified Andrade-type equation may well represent the dynamic viscosity not too close to the critical point—and some authors have simply adopted this approach for the kinematic viscosity—this type of equation fails to reasonably represent the liquid kinematic viscosity for the complete temperature range studied in the present investigation. Thus, we have chosen an empirical polynomial approach,

$$\nu' = \sum_{i=0}^{3} \nu'_i (T/\mathrm{K})^i, \tag{18}$$

Table V. Liquid Kinematic Viscosity ν' and Surface Tension σ of R410A and R407C Under Saturation Conditions[a]

T (K)	η'' (μPa·s)	ρ' (kg·m^{-3})	ρ'' (kg·m^{-3})	ν' (mm^2·s^{-1})	σ (mN·m^{-1})
			R410A		
243.15	10.8	1282.9	10.6	0.1955	13.20
253.15	11.3	1248.2	15.5	0.1740	11.61
263.15	11.8	1211.7	22.0	0.1588	10.13
273.15	12.3	1173.0	30.6	0.1461	8.66
283.15	12.9	1131.6	42.0	0.1319	7.19
293.15	13.5	1086.8	56.9	0.1214	5.78
303.15	14.2	1037.0	76.7	0.1091	4.44
313.15	15.1	980.4	103.5	0.0990	3.14
323.15	16.3	912.4	141.5	0.0910	1.93
328.15	17.2	871.4	167.5	0.0850	1.38
333.15	18.3	822.3	201.4	0.0801	0.849
338.15	19.9	757.3	250.7	0.0741	0.392
			R407C		
243.15	10.1	1339.5	6.3	0.2462	14.40
248.15	10.3	1323.3	7.8	0.2350	13.67
253.15	10.5	1306.9	9.5	0.2206	12.92
258.15	10.8	1290.0	11.6	0.2082	12.17
263.15	11.0	1272.8	14.0	0.1979	11.41
268.15	11.2	1255.1	16.7	0.1886	10.73
273.15	11.4	1237.0	19.9	0.1785	9.94
278.15	11.7	1218.4	23.5	0.1677	9.24
283.15	11.9	1199.2	27.7	0.1616	8.59
288.15	12.2	1179.4	32.5	0.1530	7.85
293.15	12.4	1158.9	37.9	0.1449	7.16
298.15	12.7	1137.7	44.2	0.1380	6.50
303.15	13.0	1115.5	51.3	0.1297	5.84
308.15	13.3	1092.2	59.4	0.1240	5.22
313.15	13.6	1067.7	68.8	0.1195	4.57
318.15	14.0	1041.6	79.5	0.1125	3.93
323.15	14.4	1013.7	92.0	0.1080	3.35
328.15	14.8	983.5	106.7	0.1025	2.75
333.15	15.4	950.4	124.0	0.0977	2.19
338.15	16.0	913.2	144.9	0.0914	1.65
343.15	16.8	870.6	170.9	0.0876	1.16
348.15	17.9	820.2	204.6	0.0823	0.696
353.15	19.4	757.6	253.2	0.0776	0.301

[a] Directly measured values for frequency ω and damping Γ at a defined wave vector q of surface waves were combined with literature data for η'', ρ', and ρ'' from Ref. 19 to derive ν' and σ by an exact numerical solution of the dispersion relation.

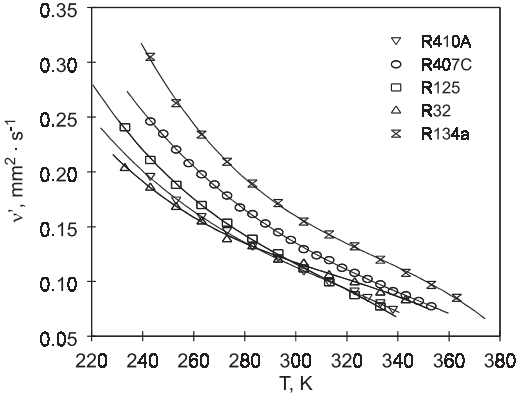

Fig. 8. Liquid kinematic viscosity of saturated R410A and R407C in comparison with the values of the pure components R32, R125, and R134a [11, 23].

to represent our experimental mixture kinematic viscosity data. The experimental data for the surface tension can well be represented by a modified van der Waals-type surface tension equation of the form [24]

$$\sigma = \sigma_0 (1 - T_R)^{1.26} [1 + \sigma_1 (1 - T_R)^{0.5} + \sigma_2 (1 - T_R)]. \tag{19}$$

In Eq. (19), σ_0, σ_1, and σ_2 are fit parameters. The critical temperatures of R410A and R407C were again obtained by visual observation and by a mass-weighted calculation scheme, respectively; see above. For R410A and

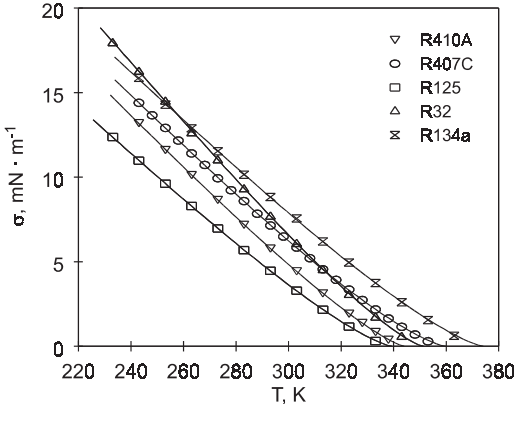

Fig. 9. Surface tension of R410A and R407C under saturation conditions in comparison with the values of the pure components R32, R125, and R134a [11, 23].

Table VI. Coefficients of Eq. (18) for R410A and R407C

ν_i' ($mm^2 \cdot s^{-1}$)	R410A	R407C
ν_0'	2.51768	2.65733
ν_1'	−0.02104374	−0.020183
ν_2'	6.360746×10^{-5}	5.4983×10^{-5}
ν_3'	-6.725671×10^{-8}	-5.2433×10^{-8}
rms (%)	0.69	0.51
T-range (K)	243–333	243–353

R407C the coefficients of Eqs. (18) and (19) are given in Tables VI and VII, respectively. Here, the standard deviations of our data relative to those calculated are also listed.

In Figs. 10 and 11 the results for liquid kinematic viscosity and surface tension, respectively, are also compared with the simple prediction method according to Eq. (17). To this end, data for the pure components were taken from previous measurements by surface light scattering [11, 23]. As can be seen from the deviation plots, the mixture results for the kinematic viscosity and surface tension follow quite well a mass-weighted calculation scheme according to Eq. (17). In addition, in Fig. 10 our viscosity values are compared with measurements by Heide and Schenk [25], which were performed by a falling-ball viscometer with a claimed uncertainty of 2%, and with values from the NIST reference database [19]. With the exception of the region close to the critical point of R410A ($T > 325$ K), where for the value given by Heide and Schenk [25] a positive deviation of 11.3% with respect to our data can be found, the data sets for the viscosity of R410A are consistent. In contrast, for R407C at low temperatures a systematic negative deviation from our values can be found for the data given by Heide and Schenk [25] and also for the data from the NIST reference database [19]. In approaching the critical point, these two data sets come closer to our data. Also, our values for the surface tension are compared

Table VII. Coefficients of Eq. (19) for R410A and R407C

	R410A	R407C
σ_0 ($mN \cdot m^{-1}$)	67.468	48.206
σ_1	−0.051	1.049
σ_2	−0.193	−1.123
rms (%)	0.76	3.8
T-range (K)	243-T_C	243-T_C

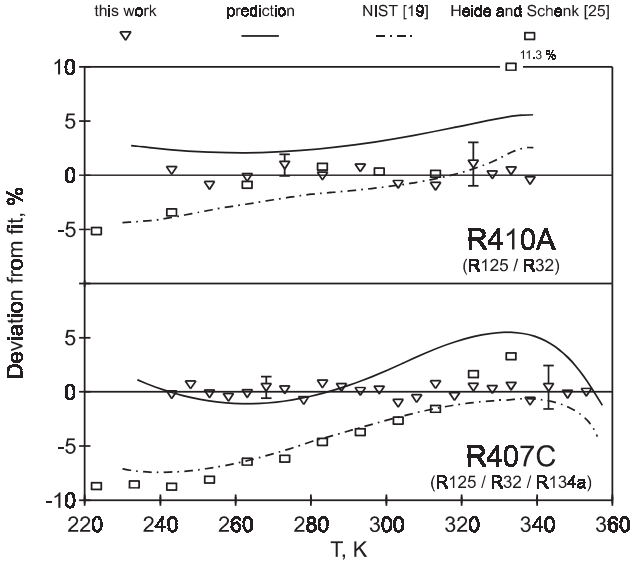

Fig. 10. Data comparisons for the liquid kinematic viscosity under saturation conditions for the binary mixture R410A and ternary mixture R407C.

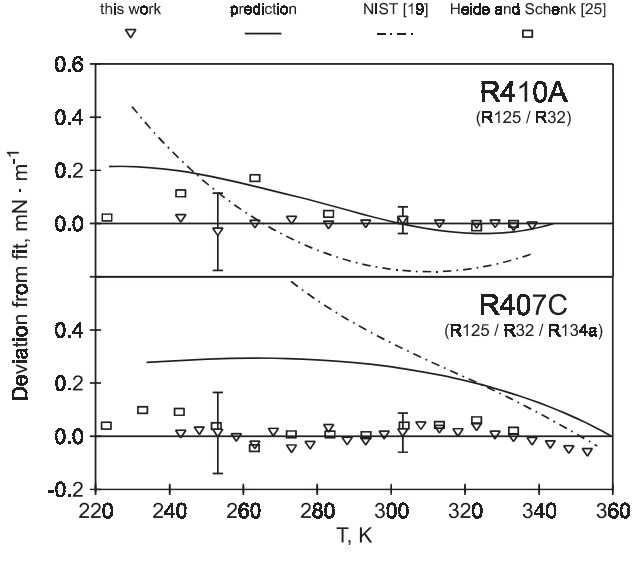

Fig. 11. Data comparisons for the surface tension under saturation conditions for the binary mixture R410A and ternary mixture R407C.

with available reference data in Fig. 11. Besides values from the NIST reference database [19], data based on measurements of the capillary rise method of Heide and Schenk [25] are included, where the stated error in measuring the surface tension, when neglecting possible density errors, amounts to $\leqslant 1\%$ for a surface tension of $10\,\mathrm{mN \cdot m^{-1}}$. Within the combined uncertainty, good agreement between our surface tension data and those of Heide and Schenk [25] can be found for the complete temperature range studied in this work.

5. CONCLUSIONS

In the present study the DLS technique has been applied successfully to the investigation of several thermophysical properties of the refrigerant mixtures R410A and R407C over a wide temperature range along the saturation line approaching the vapor-liquid critical point. Light scattering from bulk fluids has been used for the determination of thermal diffusivity and sound speed. While the investigations of these properties for the ternary zeotropic mixture R407C were restricted to the liquid phase, the binary near-azeotropic mixture R410A has been investigated also in the vapor phase. In addition, light scattering by thermally excited capillary waves on a gas-liquid interface has been used for the simultaneous determination of liquid kinematic viscosity and surface tension.

This work is the second where several thermophysical properties of refrigerant mixtures of technical interest have been measured by dynamic light scattering. The other work was done about two years ago for the binary mixture R507 and the ternary mixture R404A. The experimental results for these mixtures have already suggested that the mixture data can be accurately represented by a mass-weighted sum of the pure component data expressed as functions of the reduced temperature. Even if the same statement holds for the present work, the accuracy of the predictive approach here is less than for the refrigerant mixtures investigated in the previous work. The reason for this behavior may be found in the composition of different derivatives for R410A and R407C. While R507 and R404A are composed of only derivatives of ethane, in the present work, with R32 as a pure component of R410A and R407C, a derivative of methane also has to be taken into account.

In order to examine the simple prediction scheme based on the properties of the pure components as functions of the reduced temperature in more detail, further experimental and theoretical work is necessary. In future work we intend to investigate also mixtures with quite disparate components to find out under what circumstances the approach fails and when it can be successfully applied.

ACKNOWLEDGMENTS

The investigated refrigerants have been provided by Solvay Fluor & Derivate GmbH, Hannover. Parts of the work were supported by the Max-Buchner-Forschungsstiftung.

REFERENCES

1. A. P. Fröba, S. Will, and A. Leipertz, *Int. J. Thermophys.* **22**:1349 (2001).
2. H. Buchwald, J. Hellmann, H. König, and C. Meurer, SOLKANE® *Taschenbuch Kälte- und Klimatechnik*, Solvay Fluor & Derivate GmbH, ed. (Hannover, 1997).
3. B. Chu, *Laser Light Scattering* (Academic Press, New York, 1991).
4. D. Langevin, *Light Scattering by Liquid Surfaces and Complementary Techniques* (Marcel Dekker, New York, 1992).
5. A. Leipertz and A. P. Fröba, in *Diffusion in Condensed Matter*, J. Kärger, P. Heitjans, and R. Haberlandt, eds. (Springer, Heidelberg), in press.
6. J. W. Schmidt and M. R. Moldover, *J. Chem. Eng. Data* **39**:39 (1994).
7. J. W. Schmidt, E. Carrillo-Nava, and M. R. Moldover, *Fluid Phase Equilib.* **122**:187 (1996).
8. J. Yata, M. Hori, and T. Minamiyama, *Proc. 11th Jap. Symp. Thermophys. Prop.* (1990), pp. 111–114.
9. A. P. Fröba, S. Will, and A. Leipertz, *Fluid Phase Equilib.* **161**:337 (1999).
10. A. P. Fröba and A. Leipertz, *Int. J. Thermophys.* **24**:895 (2003).
11. A. P. Fröba, Dr.-Ing. Thesis, Friedrich-Alexander-Universität Erlangen-Nürnberg, Erlangen (2002).
12. K. Kraft and A. Leipertz, *Fluid Phase Equilib.* **125**:245 (1996).
13. K. Kraft and A. Leipertz, *Int. J. Thermophys.* **15**:387 (1994).
14. K. Kraft and A. Leipertz, *Proc. Int. Conf. CFCs, The Day After* (Padova, 1994), pp. 435–442.
15. K. Kraft, Dr.-Ing. Thesis, Friedrich-Alexander-Universität Erlangen-Nürnberg, Erlangen (1995).
16. R. Tillner-Roth and H. D. Baehr, *J. Phys. Chem. Ref. Data* **23**:657 (1994).
17. S. L. Outcalt and M. O. McLinden, *Int. J. Thermophys.* **16**:79 (1995).
18. R. H. Perry, *Chemical Engineers' Handbook* (McGraw–Hill, New York, 1973).
19. *Standard Reference Database 14*, Version 4, Nat. Inst. Stds. Tech. (NIST), Boulder, Colorado (2000).
20. SOLKANE® *Refrigerant Software*, Version 2.0, SOLVAY Fluor & Derivate GmbH, Hannover (1999).
21. N. Hoffmann, K. Spindler, and E. Hahne, in *Bestimmung der Transportgrößen von HFKW*, Bericht zum AiF-Forschungsvorhaben Nr. 10044B, Heft 2: Wärmeleitfähigkeit, Forschungsrat Kältetechnik e.V., ed. (Frankfurt am Main, 1996).
22. D. Günther and D. Steimle, in *Bestimmung der Transportgrößen von HFKW*, Bericht zum AiF-Forschungsvorhaben Nr. 10044B, Heft 3: Spezifische Wärmekapazität, Forschungsrat Kältetechnik e.V., ed. (Frankfurt am Main, 1996).
23. A. P. Fröba, S. Will, and A. Leipertz, *Int. J. Thermophys.* **21**:1225 (2000).
24. C. Miqueu, D. Broseta, J. Satherley, B. Mendiboure, J. Lachaise, and A. Graciaa, *Fluid Phase Equilib.* **172**:169 (2000).
25. R. Heide and J. Schenk, in *Bestimmung der Transportgrößen von HFKW*, Bericht zum AiF-Forschungsvorhaben Nr. 10044B, Heft 1: Viskosität und Oberflächenspannung, Forschungsrat Kältetechnik e.V., ed. (Frankfurt am Main, 1996).